Radiation Measurements 141 (2021) 106521

Contents lists available at ScienceDirect

Radiation Measurements

journal homepage: http://www.elsevier.com/locate/radmeas

Thermoluminescence due to simultaneous recombination of two electrons into two-hole centers

R. Chen [a,*], J.L. Lawless [b], V. Pagonis [c]

[a] Raymond and Beverly Sackler School of Physics and Astronomy, Tel Aviv University, Tel Aviv, 69978, Israel
[b] Redwood Scientific Incorporated, Pacifica, CA, 94044-4300, USA
[c] Physics Department, McDaniel College, Westminster, MD, 21157, USA

ARTICLE INFO

Keywords:
Thermoluminescence
Two-electron transitions
Simulations
Superlinearity
High frequency factor

ABSTRACT

A model describing the possibility of simultaneous recombination of two electrons into two-hole recombination centers yielding thermoluminescence (TL) is presented. This follows previous reports on such transitions in some other solid-state phenomena. The simulated results may explain some unusual TL effects. These include the occurrence of very narrow peaks which results in the evaluation of very high effective activation energies and exceedingly high effective frequency factors, sometimes reported in the literature. The model can also explain the more-than-quadratic dose dependence of TL. Other effects are peaks with symmetry factors smaller than that of first-order peaks or intermediate between that of first and of second order. Another result of the simulations is the possibility of first-order-like peaks that shift with the excitation dose. Finally, the possibility of a dose-rate effect is also seen in the results of the simulations. In addition to the numerical simulations, limited to a small number of sets of parameters, an analytical treatment with some approximations has been developed. For a certain set of parameters and rather low excitation dose, the agreement between the results of the simulation and theory has been very good.

1. Introduction

In previous papers, Chen et al. (2017, 2018) have described TL models consisting of either a two-electron trap and a single-hole recombination center or a single-electron trap and a double-hole center. The former model explained the occurrence of two TL peaks, the first exhibiting first-order features and the second having second-order kinetics. The lower-temperature peak showed an initial steep superlinear dependence on the dose, cubic or somewhat steeper than cubic. The concepts of two-electron traps and two-hole centers had been mentioned in the literature for the explanation of different solid-state phenomena. A number of papers reported on effects associated with two-electron traps in alkali halides. Porret and Lüty (1971) reported on luminescence of F centers in KCl, and described the formation of a two-electron F′ center. Baldacchini et al. (1981) communicated on radiative and non-radiative processes of F and F′ centers in NaBr and NaI, concentrating on the role of two-electronic states. Zhang et al. (1994) also discussed the two-electron systems in ionic crystals, and in particular, the role of F′ centers in alkali-halides. Woda and Wagner (2007), in an explanation of a non-monotonic dose dependence of Ge- and Ti-centers in quartz, discussed a model of double-electron capture which can explain the effect in both ESR and TL measurements.

A quite similar situation of two-hole centers has been considered in the literature. Winter et al. (1969) reported on the dichroism of V bands in potassium and rubidium halides and explained the results using a model of two holes trapped at an anion in a cation vacancy. Dean et al. (1967) reported on two-electron transitions in the luminescence of gallium phosphide. The authors state that in this material, the two-electron luminescence lines are weak, and for them to be seen, crystals must be prepared in such a way that other luminescence emissions must be of low intensity. More specifically, with regard to TL, Mayhugh (1970) and Townsend et al. (1979) explained results of thermoluminescence in LiF by the existence of V_3 centers containing two trapped holes. Böhm and Scharmann (1981) mentioned the two-electron F′ center in alkali-halides with relation to the general subject of TL dosimetry. Yazici et al. (2004) who studied TL of LiF:Mg, Ti between 100 and 300 K suggested that their results are related to the V_3 two-hole centers. The same V_3 two-hole centers have been considered as being associated with TL by Horowitz (2006) and by Eliyahu et al. (2016). Horowitz et al. (2018) have given a review on the dose-rate effects in TL

* Corresponding author.
E-mail address: chenr@tau.ac.il (R. Chen).

https://doi.org/10.1016/j.radmeas.2021.106521
Received 22 October 2020; Received in revised form 10 December 2020; Accepted 11 January 2021
Available online 19 January 2021

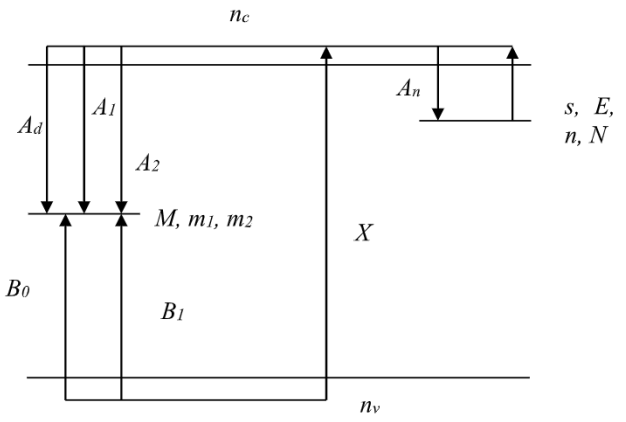

Fig. 1. Energy-level diagram of a model with an electron trap and a two-hole recombination center. The meaning of the different variables is given in the text.

of LiF:Mg, Ti and tentatively associated it with the two-hole capture in V_3 centers.

In a later paper, Chen et al. (2018) have studied theoretically the TL model with two-hole centers when the recombination of two electrons from the conduction band takes place sequentially. In the present work, we consider another possibility in which instead of or in addition to the sequential recombination, a simultaneous recombination of two electrons from the conduction band can take place with the two trapped holes in the center.

It deserves mention that several previous works described the possibility of simultaneous two-electron-one photon recombination which explained other than TL solid-state phenomena. Betzler and Weller (1971) and Betzler et al. (1972) explained the emission at $h\nu=2E_g$ where E_g is the band gap in Si by two-electron radiative transition across the band gap. As could be expected, the intensity of the effect depended quadratically on the excitation intensity. Berezin (1984) considered a system of two neutral and two negatively charged impurity atoms in a semiconductor. For certain configurations of this array all one-electron transitions would violate the energy-conservation law. However, the system can spontaneously make a transition to a lower energy state by simultaneous tunnel transitions of both electrons. The author mentions the extreme case where all one-electron tunnelings are prohibited while two-electron correlated jumps are allowed. Wagner et al. (1992) reported on two-electron transitions (TETs) and two-hole transitions (THTs) which are possible in ZnTe layers. Burbaev et al. (2013) communicated on low-temperature photoluminescence of Si/SiGe/Si heterostructures, resulting from simultaneous recombination of four particles, two electrons and two holes.

In the present work we offer a TL model of an electron trap and a hole recombination center, the latter capable of capturing two holes with the additional feature that simultaneous two-electron transition may take place from the conduction band into the two-hole center. An important point is to be made with regard to the terms associated with the two-electron simultaneous transition which should be added to the relevant set of simultaneous equations governing the process during the excitation and the read-out. Whereas the single-electron transitions required the use of terms linear in the concentration of free electrons in the conduction band (n_c), the situation here is different and quadratic terms in n_c must be used in the rate equations as elaborated below. A recent paper by Lawless et al. (2019) has also used a set of differential equations with a quadratic term in n_c while dealing with another possible thermoluminescence effect associated with an Auger-recombination process.

Some TL effects that can be explained by this model are steep superlinear dose dependence of the intensity as well as different possible symmetries of the TL peak including unusual ones having an effective order smaller than unity. The model can also explain the occurrence of extremely high effective frequency factors that are sometimes evaluated. Finally, a demonstration of a possible dose-rate effect is shown.

In the simulations as well as in the analytical approach with approximations, we will distinguish between cases of high, low and intermediate recombination probability coefficients of the simultaneous two-electron transition which will show different possible features of the resulting TL peaks.

2. The model

The following model deals with one trap, N (cm^{-3}), with an instantaneous occupancy of n (cm^{-3}) and one center, M (cm^{-3}), which may trap either one or two holes during excitation by irradiation. A schematic energy-level diagram of the model is shown in Fig. 1. The activation energy of electrons thermally raised into the conduction band is E (eV) and the frequency factor is s (s^{-1}). The retrapping probability coefficient of an electron from the conduction band back to the trap is A_n (cm^3s^{-1}). m_1 (cm^{-3}) is the instantaneous concentration of centers holding one hole and m_2 (cm^{-3}) is the concentration of centers with two holes. B_0 (cm^3s^{-1}) is the probability coefficient for trapping a hole in a neutral center and B_1 (cm^3s^{-1}) is the probability coefficient for trapping a hole in a center occupied by one hole. A_1 (cm^3s^{-1}) is the recombination probability coefficient of a free electron into a center occupied by a single hole and A_2 (cm^3s^{-1}) is the recombination probability coefficient into a center with two holes. A_d (cm^6s^{-1}) is the probability coefficient of the simultaneous recombination of two electrons from the conduction band into the two-hole center. X ($cm^{-3}s^{-1}$) is the rate of production of electron-hole pairs by the irradiation, proportional to the dose rate. If the irradiation takes place during a time t_D (s), then $D=X\cdot t_D$ (cm^{-3}) is the total concentration of pairs produced, per unit volume, proportional to the total applied dose. n_c (cm^{-3}) and n_v (cm^{-3}) are respectively the instantaneous concentrations of free electrons and free holes.

The equations governing the process during excitation are:

$$\frac{dn}{dt}=A_n(N-n)n_c-sn\exp(-E/kT), \tag{1}$$

$$\frac{dm_1}{dt}=B_0n_v(M-m_1-m_2)-B_1m_1n_v-A_1n_cm_1+A_2n_cm_2, \tag{2}$$

$$\frac{dm_2}{dt}=B_1m_1n_v-A_2n_cm_2-A_dn_c^2m_2, \tag{3}$$

$$\frac{dn_v}{dt}=X-B_0(M-m_1-m_2)n_v-B_1m_1n_v, \tag{4}$$

$$\frac{dn_c}{dt}=X-A_n(N-n)n_c-A_1m_1n_c-A_2m_2n_c+s\cdot n\cdot\exp(-E/kT)-2A_dn_c^2m_2. \tag{5}$$

Note the last terms in Eqs. (3) and (5). These are the additional terms to those used by Chen et al. (2018) for the sequential recombination of two electrons in the two-hole center. The additional term here considers the simultaneous two-electron transition into the two-hole center. In full analogy to the law of mass action, dealing with the rate equations of chemical reactions (Guldberg and Waage, 1864; Lund, 1965; Hinkley and Tsokos, 1974; Baird, 1999; Ferner and Aronson, 2016), the relevant term for the simultaneous recombination of two electrons should be proportional to n_c^2 but linear with the concentration of the two-hole centers, hence the $m_2n_c^2$ term. The occurrence of this term, quadratic in n_c, is very similar to that described by Lawless et al. (2019) for the Auger recombination process. The similarity between the two models has to do with the simultaneous involvement of two electrons in the recombination process. Note also the coefficient of 2 in front of this term in Eq. (5). Whereas in Eq. (3), the rate of change is of m_2, the concentration of the two-hole occupied center, Eq. (5) deals with the

concentration of free electrons, hence the multiplication by 2 (see also Chen et al., 2018). Due to the nature of this last term in Eqs. (3) and (5), obviously, the units of the coefficient A_d are cm^6s^{-1} as pointed out above, and its size cannot be directly compared to that of A_1, A_2 and A_n. It should be mentioned that we have included in the equations both the sequential recombination of two electrons into the two-hole center and the simultaneous two-electron coefficient. Simulation parameters can be chosen so that either the sequential or simultaneous processes dominate or that both are important.

Let us apply the initial conditions $m_1(0) = m_2(0) = n(0) = 0$ and we get from Eqs. (1)–(5)

$$n_c + n = n_v + m_1 + 2m_2. \tag{6}$$

Note that Eq. (6) is a charge balance condition. The factor of 2 in front of m_2 indicates that, instantaneously, m_2 centers hold two holes each. Equation (6) can be written in a differential way as

$$\frac{dn_c}{dt} = \frac{dm_1}{dt} + 2\frac{dm_2}{dt} + \frac{dn_v}{dt} - \frac{dn}{dt}. \tag{7}$$

If one wishes to simulate the TL process, it has to be done, as usual, in three stages. A set of parameters is to be chosen with a certain dose rate X and Eqs. (1)–(5) solved numerically for a certain period of time t_D. In the next stage of relaxation, one should set $X = 0$, use the last values of the first stage as initial values for the second stage and solve the same equations for a certain period of time so that n_c and n_v are reduced to practically zero. In the last stage of heating, a certain heating function $T=T(t)$ is to be chosen, usually a linear function $T=T_0+\beta t$ is used where β (Ks^{-1}) is the constant heating rate. The last values of the concentration functions in the second stage are to be used as initial values for the third stage. Also, X is kept zero and therefore, at this stage, $n_v \equiv 0$ thus, Eq. (4) can be ignored at this stage.

3. Numerical simulations and results

As can be understood from the discussion above and Eqs. (1)–(5), the expected TL depends on several parameters. The simultaneous-two-electron recombination probability coefficient A_d is, of course, of great importance, but the magnitude of the other parameters, namely, A_1, A_2, A_n, B_0, B_1, s, E, M and N may influence significantly the results. Also, the excitation dose rate, X and the time of excitation t_D are important. In the following report of simulations and approximate analytical treatment we can show only examples that will cover effects such as the dose dependence for certain choices of the set of other parameters or the dependence of the TL on the probability coefficient A_d when the other parameters are kept constant. As shown below, unusual effects such as nonlinear dose dependence or high effective activation energies and very high apparent frequency factors, can be explained by the model and the set of equations (1)–(5). It is worth mentioning that the present model is a possible alternative to other models which can explain the occurrence of very high effective frequency factors; this point is mentioned in the Discussion below.

As pointed out before (Chen et al., 2018) the probability of capturing the second hole in the center is expected to be smaller than that of the first hole, $B_0 > B_1$, due to Coulombic repulsion. Also, one expects that $A_2 > A_1$ since the Coulombic attraction of a free electron is stronger for transitions into a center with two holes than into one with a single hole. The emission of light can be associated with, $A_d m_2 n_c^2$, $A_2 m_2 n_c$, $A_1 m_1 n_c$ or some weighted sum of them. Let us denote the three emission peaks by $I_3(T)$, $I_2(T)$ and $I_1(T)$ associated with the recombination of a free electron with a center with two-holes simultaneously, recombination of a single electron with a two-hole center and a recombination of an electron with a one-hole center, respectively. These three intensities are given by

$$I_3(T) = A_d m_2 n_c^2, \tag{8}$$

$$I_2(T) = A_2 m_2 n_c, \tag{9}$$

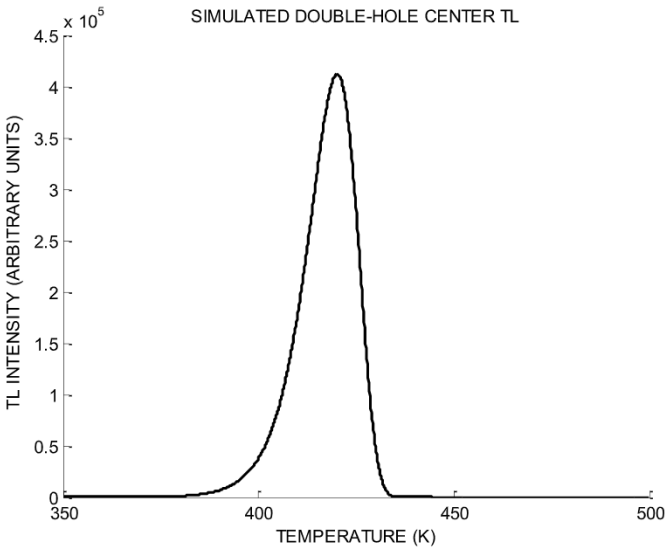

Fig. 2. Simulated TL peak associated with the double-electron transition. The parameters are given in the text and $A_d = 10^{-16}\ cm^6s^{-1}$ and $t_D = 1.0$ s. The peak is seen to be asymmetric, and analysis shows it has a symmetry factor of $\mu_g = 0.408$.

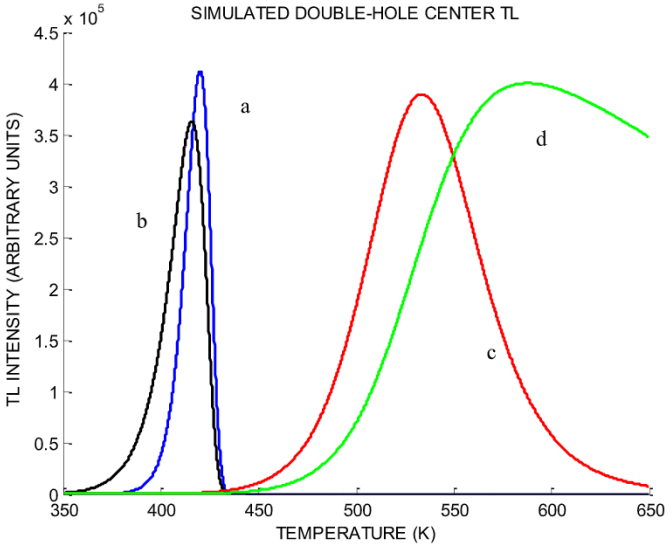

Fig. 3. Simulated TL associated with the three possible transitions: (a) $I_3 = A_d m_2 n_c^2$, (b) $(300) I_2 = A_2 m_2 n_c$ and (c) $(3 \times 10^{-7}) I_1 = A_1 m_1 n_c$ and (d) shows the dependence of n_c on temperature. The set of parameters used is the same as in Fig. 2.

and

$$I_1(T) = A_1 m_1 n_c, \tag{10}$$

Note that these three transitions may have different emission spectra. In the following, we will concentrate mainly on $I_3(T)$. In some cases we choose $A_1 = 0$, which, of course, yields $I_1(T) \equiv 0$, and anyway, we assume that $I_3(T)$ can be separated spectrally from the other two emissions if they take place or if they are radiationless.

The parameters used for the simulations were:

$B_0 = 10^{-11}\ cm^3s^{-1}$; $B_1 = 10^{-12}\ cm^3s^{-1}$; $A_n = 10^{-13}\ cm^3s^{-1}$; $A_1 = 10^{-12}\ cm^3s^{-1}$; $A_2 = 10^{-11}\ cm^3s^{-1}$; $A_d = 10^{-16}\ cm^6s^{-1}$; $s = 10^{12}\ s^{-1}$; $E = 1.2$ eV; $N = 10^{17}\ cm^{-3}$; $M = 10^{16}\ cm^{-3}$ and the heating rate was $\beta = 1$ K/s. The dose rate X was set at $10^{14}\ cm^{-3}s^{-1}$ and the time of excitation $t_D = 1$ s. Fig. 2 shows the results of the simulations as received by the

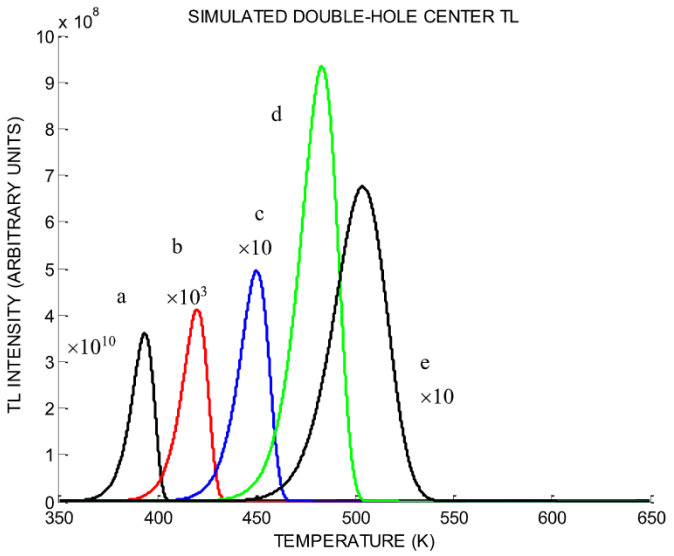

Fig. 4. TL peaks simulated with the parameters mentioned in the text and (a) $A_d = 10^{-14}$ cm^{6}s^{-1}; (b) $A_d = 10^{-16}$ cm^{6}s^{-1}; (c) $A_d = 10^{-18}$ cm^{6}s^{-1}; (d) $A_d = 10^{-20}$ cm^{6}s^{-1}; (e) $A_d = 10^{-22}$ cm^{6}s^{-1}. The intensities are multiplied by the factors given in the text and shown on the figure.

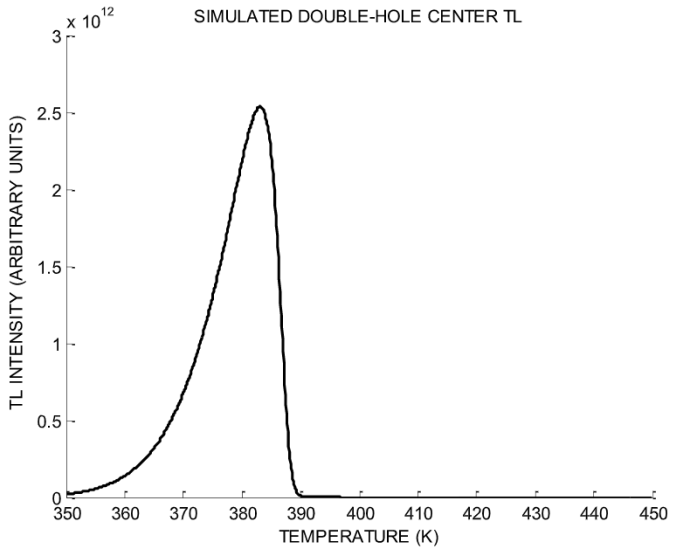

Fig. 5. Simulated glow peak with the same parameters as in Fig. 2, but the excitation dose is much higher with $X = 3.2 \times 10^{15}$ cm^{-3}s^{-1} and $t_D = 10$ s. The peak looks skewed with $\mu_g = 0.288$.

numerical solution of Eqs. (1)–(5) in the three stages of excitation, relaxation and heating. The equations were solved by the MATLAB ode15s solver. The shown peak, found by Eq. (8), has been analyzed using the peak-shape method (see e.g., Chen, 1969). The symmetry factor has been found to be $\mu_g = 0.408$, indicating an effective order of kinetics slightly smaller than one. The effective activation energy found has been $E_{eff} = 2.33$ eV and the evaluated frequency factor $s_{eff} = 1.21 \times 10^{27}$ s^{-1}. These values will be discussed below.

As pointed out above, the other two transitions, given by Eqs. (9) and (10) may also contribute to the emitted TL. Fig. 3 shows the three possible simulated peaks. Curve (a) is the same two-hole transition peak as in Fig. 2, curve (b) has been found by Eq. (9), showing the transitions of single electrons into hole centers with two trapped hole and curve (c) shows the TL associated with the transition of single electrons into a single-charged hole center, associated with Eq. (10). In order to show all these peaks on the same graph, the intensity of curve (b) has been multiplied by 300 and of curve (c) by 3×10^{-7}. Of course, with different sets of parameters, the relative intensities of the peaks may be significantly different. Curve (d) shows the simulated curve of $n_c(T)$. As stated before (see e.g., Chen, 1971), the rule that TL peaks occur at lower temperatures than the relevant $n_c(T)$ peak takes place here for all the three TL peaks. Note that the symmetry factor of curve (c) is ~0.52, typical of second-order peaks.

An interesting point to study has been the variation of the simulated TL peak with the size of the double-electron transition probability coefficient A_d when the other parameters are kept constant. Some results are shown in Fig. 4. The parameters used are those mentioned above. Curve (a) was found with $A_d = 10^{-14}$ cm^{6}s^{-1}; (b) $A_d = 10^{-16}$ cm^{6}s^{-1}; (c) $A_d = 10^{-18}$ cm^{6}s^{-1}; (d) $A_d = 10^{-20}$ cm^{6}s^{-1}; (e) $A_d = 10^{-22}$ cm^{6}s^{-1}. The peaks are seen to shift quite significantly to higher temperatures with decreasing values of A_d, roughly by ~15 K for an order of magnitude decrease in A_d. The peaks look like first-order curves with the symmetry factor of ~0.41, which increases to ~0.46 with the lowest value of A_d which implies the occurrence of an intermediate effective order of kinetics. The peaks are very narrow, and using the peak-shape method (Chen, 1969), the effective activation energy is ~1.9–2.33 eV, up to nearly twice the value of 1.2 eV inserted into the simulation. The effective frequency factor is in the range of 10^{18}-10^{29} s^{-1} many orders of magnitude higher than the inserted value. These results will be discussed below. A rather surprising result is that as shown in curves (a-d), the peaks' intensities increase for decreasing values of A_d. This will also be discussed below.

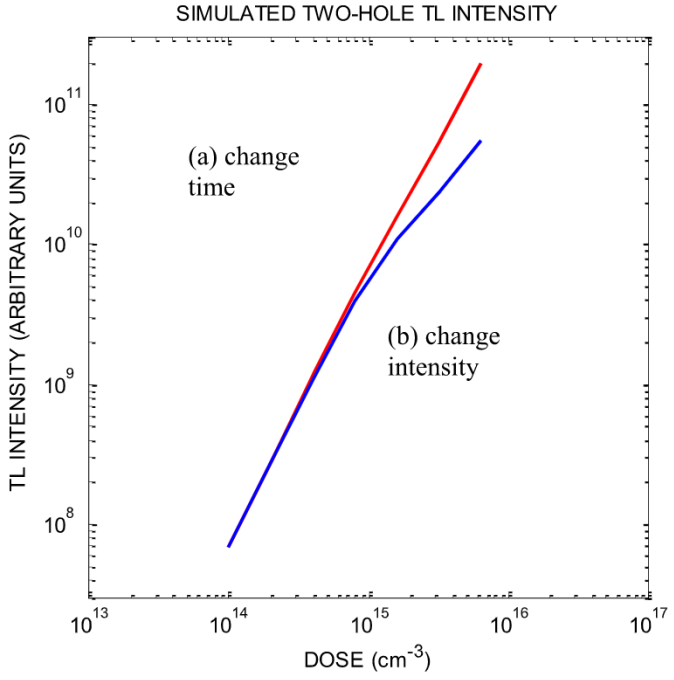

Fig. 6. Simulated dose dependence of the TL maximum intensity. The parameters used were the same as in Fig. 2. Curve (a) describes the results with constant intensity of excitation X and variable time of excitation t_D and curve (b) shows the results with constant time and variable intensity.

Fig. 5 presents a simulated glow peak with rather unusual features. The parameters are the same as in Fig. 2, but the excitation dose is much higher with $X = 3.2 \times 10^{15}$ cm^{-3}s^{-1} and $t_D = 10$ s. The peak looks skewed with $\mu_g = 0.288$. Such unusual results were reported in the literature as discussed below.

Another interesting feature of the results is the very strong supralinearity of the TL intensity. An example of the dependence on the dose of excitation of I_{3m}, the maximum intensity of I_3, is shown in Fig. 6. The parameters are the same as above with $A_d = 10^{-22}$ cm^{6}s^{-1} and t_D varies

from 1 to 64 s. Practically the same superlinear results were reached by varying the dose rate, keeping the time of excitation constant at relatively low doses. At higher doses, the two lines split and the time-change line is higher. This indicates a dose-rate effect. The superlinear dose dependence will be discussed below. It is interesting to note that although the peaks look like being of first order, they shift to lower temperature with increasing dose. In the mentioned dose range between 10^{14} and 6.4×10^{15} cm^{-3}, the shift was by ~42.6 K, from 492.8 K to 450.2 K.

4. Approximate analytical theory

4.1. Irradiation

If we assume that the lifetimes for free electrons and free holes are small compared to the timescales for either irradiation or heating and that A_d is small enough that

$$2A_d n_c m_2 << A_n N, \tag{11}$$

then Eqs. (4) and (5) reduce to

$$n_v = \frac{X}{B_0(M - m_1 - m_2) + B_1 m_1}, \tag{12}$$

$$n_c = \frac{X + ns\exp(-E/kT)}{A_n(N-n) + A_1 m_1 + A_2 m_2}. \tag{13}$$

For initial conditions, we assume the trap and center to be empty,

$$n = 0; \quad m_1 = 0; \quad m_2 = 0, \tag{14}$$

at $t = 0$. For low dose, the trap and center populations will remain small that

$$n << N; \quad A_1 m_1 + A_2 m_2 << A_n N, \tag{15}$$

$$m_1, m_2 << M, \tag{16}$$

$$B_1 m_1 << B_0 M. \tag{17}$$

For irradiation, we further neglect thermal excitation and Eqs. (12) and (13) then simplify to

$$n_c = \frac{X}{AN}, \tag{18}$$

$$n_v = \frac{X}{B_0 M}. \tag{19}$$

Under these approximations, Eqs. (2) and (3) simplify to

$$\frac{dm_1}{dt} = X, \tag{20}$$

$$\frac{dm_2}{dt} = \frac{B_1 m_1}{B_0 M} X - \left(A_2 + A_d \frac{X}{A_n N}\right) \frac{X}{A_n N} m_2. \tag{21}$$

Equation (20) is readily integrated to find m_1 at the end of irradiation,

$$m_1 = \int_0^{t_D} X dt \equiv D, \tag{22}$$

where t_D is the duration of irradiation, D is the dose (expressed as created electron-hole pairs per unit volume).

Note that because of the low dose assumption, specifically Eq. (17), it follows from Eqs. (20) and (21) that $m_2 << m_1$.

From Eq. (21), we see that the lifetime of state m_2 is

$$\tau_{m_2} = \frac{1}{\left(A_2 + A_d \frac{X}{A_n N}\right) \frac{X}{A_n N}}. \tag{23}$$

If this lifetime is small compared to the time scales of irradiation and heating, as it is for the parameters used in Fig. 2, then the concentration of m_2 becomes quasi-steady with the value

$$m_2 = \frac{B_1 m_1 X/(B_0 M)}{\left(A_2 + A_d \frac{X}{A_n N}\right) \frac{X}{A_n N}}. \tag{24}$$

If we further assume, as in the case of Fig. 2, that $A_2 << A_d \frac{X}{A_n N}$, then Eq. (24) simplifies to

$$m_2 = \frac{B_1 A_n^2 N^2}{A_d B_0 M} \frac{m_1}{X}. \tag{25}$$

If X is independent of time, as in our simulations, then, subject to the assumed parameter ranges as above, m_2, is proportional to time t, as per Eq. (22), and has the peculiar property of being independent of X,

$$m_2 = \frac{B_1 A_n^2 N^2}{A_d B_0 M} t. \tag{26}$$

In sum, the values of m_1 and m_2 at the end of irradiation are found to be given by Eqs. (22) and (24). Since $m_2 << m_1$, the trap concentration is $n \approx m_1$.

4.2. Relaxation

Since $n_c \ll m_1$, the population m_1 remains practically unchanged during heating. For m_2, the reverse is true and the population of m_2 after relaxation depends on the process by which n_c and n_v decay. It will be easy to determine the profiles of n_c and n_v during relaxation. Determining m_2 will take some math.

We consider the case where irradiation, X, suddenly drops to zero at t_D. (If the drop is not sudden, we would need a different theory). Thus, for $t > t_D$, Eqs. (3)–(5) reduce to

$$\frac{dm_2}{dt} = B_1 m_1 n_v - A_d n_c^2 m_2, \tag{27}$$

$$\frac{dn_v}{dt} = -B_0 M n_v, \tag{28}$$

$$\frac{dn_c}{dt} = -A_n N n_c. \tag{29}$$

The conditions at the end of irradiation are the initial conditions for relaxation,

$$m_{2D} = \frac{B_1 A_n^2 N^2 m_1}{A_d B_0 M} \frac{m_1}{X_D}; \quad n_{cD} = \frac{X_D}{A_n N}; \quad n_{vD} = \frac{X_D}{B_0 M}, \tag{30}$$

where the subscript D indicates that these are values at time t_D just before the irradiation terminates. Equations (28) and (29) are readily integrated. For $t > t_D$,

$$n_v = n_{vD} e^{-B_0 M (t - t_D)}, \tag{31}$$

$$n_c = n_{cD} e^{-A_n N (t - t_D)}. \tag{32}$$

With these solutions, Eq. (27) becomes

$$\frac{dm_2}{dt} = B_1 m_1 n_{vD} e^{-B_0 M (t - t_D)} - A_d n_{cD}^2 e^{-2A_n N (t - t_D)} m_2. \tag{33}$$

There are two time scales of particular importance in Eq. (33). The first is $1/(B_0 M)$ which is the e-folding time scale for n_v. For the parameters in Fig. 2 this is 10 μs. The second is $1/(2A_n N)$ which is the e-folding time for n_c. For the same set of parameters this is 50 μs. Because the former is much smaller than the latter, we can solve Eq. (33) in two steps. One involves the short time scale over which n_v decays and the other occurs over the longer time scale over which n_c decays.

Since our primary interest is in knowing the conditions at the end of relaxation, let us first look at the longer time scale, $(t\text{-}t_D) \gg 1/(B_0 M)$. In

this case, Eq. (33) simplifies to

$$\frac{dm_2}{dt} = -A_d n_{cD}^2 e^{2A_n N(t-t_D)} m_2. \tag{34}$$

After some math, the solution of Eq. (34) is found to be

$$m_2 = C\exp\left\{-\frac{A_d n_c n_{cD}^2}{2A_n N}[1-\exp(-2A_n N(t-t_D))]\right\}, \tag{35}$$

where C is a constant of integration. To find C, we need a solution for Eq. (33) that is accurate for short times and whose validity overlaps that of Eq. (35).

For shorter time scales, $0<t\text{-}t_D \ll 1/(2A_nN)$, Eq. (33) simplifies to

$$\frac{dm_2}{dt} = B_1 m_1 n_{vD} e^{-B_0 M(t-t_D)} - A_d n_{cD}^2 m_2. \tag{36}$$

This is a linear first-order equation and can be immediately integrated to find

$$m_2 = m_{2D} e^{-A_d n_c D^2 (t-t_D)} + \frac{B_1 m_1 n_{vD}}{B_0 M - A_d n_{cD}^2}\left(e^{-A_d n_c D^2 (t-t_D)} - e^{-B_0 M(t-t_D)}\right). \tag{37}$$

For intermediate times, $1/(B_0M) \ll t\text{-}t_D \ll 1/(2A_nN)$, it simplifies to

$$m_2 = \left(m_{2D} + \frac{B_1 m_1 n_{vD}}{B_0 M - A_d n_c n_{cD}^2}\right) e^{-A_d n_{cD}^2 (t-t_D)}. \tag{38}$$

For these intermediate times, both Eqs. (35) and (38) are valid. Comparing the two, we find the value of C,

$$C = m_{2D} + \frac{B_1 m_1 n_{vD}}{B_0 M - A_d n_{cD}^2}. \tag{39}$$

Combining Eq. (35) with Eq. (39), our longer time-scale solution becomes

$$m_2 = \left(m_{2D} + \frac{B_1 m_1 n_{vD}}{B_0 M - A_d n_{cD}^2}\right)\exp\left\{-\frac{A_d n_{cD}^2}{2AN}[1-\exp(-2A_n N(t-t_D))]\right\}. \tag{40}$$

Since we are particularly interested in the value of m_2 at the end of relaxation, we take the $t\to\infty$ limit of Eq. (40) to find

$$m_{2C} = \left(m_{2D} + \frac{B_1 m_1 n_{vD}}{B_0 M - A_d n_{cD}^2}\right)\exp\left(-\frac{A_d n_{cD}^2}{2A_n N}\right), \tag{41}$$

where the subscript C in m_{2C} indicates the value at the end of relaxation.

The various terms in Eq. (41) which affect m_2 during relaxation can be identified as follows. m_{2D} comes from the end of irradiation. The second term in the first parentheses is the increase due to capture of free holes and the exponential term has to do with the decrease due to free electron recombination.

In sum, the solutions for n_v and n_c were found to be Eqs. (31) and (32). The final value of m_2 after the end of relaxation was found to be Eq. (41). The value of m_1 is unchanged.

4.3. Heating

Compared to relaxation, the analysis of the heating stage is relatively simple. For heating, $X = 0$, and again using the low dose approximation, Eq. (15) through (17), Eq. (13) and Eq. (12) reduce to

$$n_c = \frac{m_1 s e^{-E/kT}}{A_n N}, \tag{42}$$

$$n_v = 0. \tag{43}$$

Equations (3) and (4) then simplify to

$$\frac{dm_1}{dt} = -(A_1 m_1 - A_2 m_2)\frac{m_1 s e^{-E/kT}}{A_n N}, \tag{44}$$

$$\frac{dm_2}{dt} = -\left(A_2 + A_d \frac{m_1 s e^{-E/kT}}{A_n N}\right)\frac{m_1 s e^{-E/kT}}{A_n N} m_2. \tag{45}$$

For the low dose range, we found that after irradiation, m_2 is much smaller than m_1. Further,

$$A_2 m_2 << A_1 m_1, \tag{46}$$

and thus, Eq. (44) simplifies to

$$\frac{dm_1}{dt} = -\frac{A_1 s}{A_n N} e^{-E/kT} m_1^2. \tag{47}$$

Consequently, the emission due to $A_1 m_1 n_c$ is an ordinary second-order peak with effective pre-exponential factor of $A_1 s/(A_n N)$. Starting from the initial condition of $m_1 = m_{1D}$ and $T = T_0$ at the start of heating, the solution to Eq. (47) is

$$m_1 = \frac{m_{1D}}{1 + \frac{A_1 m_{1D} s E}{A_n N k\beta}[\Gamma(-1, E/kT) - \Gamma(-1, E/kT_0)]}, \tag{48}$$

where Γ is the incomplete gamma function,

$$\Gamma(a,x) \equiv \int_x^\infty e^{-w} w^{a-1} dw, \tag{49}$$

where w is a variable of integration.

Combining Eqs. (47) and (48), we have an equation for the free electron concentration during heating,

$$n_c = \frac{m_{1D} s \exp(-E/kT)}{A_n N + \frac{A_1 m_{1D} s E}{k\beta}[\Gamma(-1, E/kT) - \Gamma(-1, E/kT_0)]}. \tag{50}$$

Combining Eq. (10) with Eqs. (42) and (48), we have an equation for I_1,

$$I_1 = A_1 \left\{\frac{m_{1D}}{1 + \frac{A_1 m_{1D} s E}{A_n N k\beta}[\Gamma(-1, E/kT) - \Gamma(-1, E/kT_0)]}\right\}^2 \frac{s \exp(-E/kT)}{A_n N}. \tag{51}$$

For A_d sufficiently large, the second term in parentheses in Eq. (45) dominates the first and Eq. (45) simplifies to

$$\frac{dm_2}{dt} = -s_{eff,2} s^{-2E/kT} m_2, \tag{52}$$

where $s_{eff,2}$ is

$$s_{eff,2} = \frac{A_d m_1^2 s^2}{(A_n N)^2}. \tag{53}$$

This indicates that the $I_3 = A_d n_c^2 m_2$ peak behaves as a standard first-order peak, but with different effective parameters. For the conditions of Figs. 2 and 3, the effective activation energy and frequency factor are given for the set of parameters mentioned above by

$$E_{eff} = 2E = 2.4\ eV, \tag{54}$$

$$s_{eff,2} = \frac{A_d m_1^2 s^2}{(A_n N)^2} = 1 \times 10^{28} s^{-1}. \tag{55}$$

This differs somewhat from the numerical results of the peak-shape method applied to the simulated peak which yielded 2.33 eV and $1.21 \times 10^{27}\ s^{-1}$. The small differences between the respective values can be attributed to the approximations made.

To obtain $I_2 = A_2 m_2 n_c$, we will integrate Eq. (52) to find

$$m_2 = m_{2D}\exp\left(-\frac{E\, s_{eff,2}}{k\beta}\Gamma(-1, 2E/kT)\right), \tag{56}$$

where β is the heating rate.

With Eq. (56), the intensities for the two peaks associated with m_2 are immediately found,

$$I_2 = A_2 \frac{m_1 s}{A_n N} m_{2D} \exp\left(-E \Big/ kT - \frac{E\, s_{eff,2}}{k\beta} \Gamma(-1, 2E/kT) \right), \quad (57)$$

$$I_3 = s_{eff,2} m_{2D} \exp\left(-2E \Big/ kT - \frac{E\, s_{eff,2}}{k\beta} \Gamma(-1, 2E/kT) \right). \quad (58)$$

Equation (58) is, as expected, the standard equation for a first-order peak. Equation (57) does not represent a standard shape. It has an initial rise characterized by E but a tail that drops more like being associated with $2E$.

In sum, the equations for the three peaks have been found. Equation (47) shows that the peak associated with m_1 is a standard second-order peak. The peak associated with A_d, Eq. (58) is a standard first-order peak and the peak associated with A_2, given by Eq. (57) is non-standard.

5. Discussion

It appears that the possible occurrence of simultaneous two-electron transitions may explain some exotic effects reported in the literature. For example, similarly to cases of competition between two traps or centers (see e.g. Kristianpoller et al., 1974; Bowman and Chen, 1979; Chen and Fogel, 1993; Chen et al., 1996), the dose dependence of the I_3 (simultaneous two-electron transition) TL peak here is superlinear. This superlinearity is very steep, resembling the very strongly superlinear dose dependence previously reported in TL of diamonds (Halperin and Chen, 1966), CaF_2:Tb_4O_7 (Otaki et al., 1994) and quartz (Chen et al., 1988). The present explanation may be an alternative to previous accounts of superlinearity based on competition between traps or centers (see e.g. Chen et al., 1996).

The very narrow shape of the peak is of interest. As pointed out above, the peak-shape methods as well as curve fitting yield very high effective activation energy of ~2.3 eV, nearly twice as much as the inserted value of 1.2 eV, and close to the value of 2.4 eV which has been predicted by the theory. The accompanying effective frequency factor was found to be in the range of 10^{24}-10^{30} s^{-1} in the simulations and 10^{28} s^{-1} in the theory. Very high values of E and s of this sort, associated with a very narrow TL peak, have been reported in the literature. The most well-known case is peak 5, at ~210 °C, in LiF:Mg, Ti (TLD-100). Isothermal decay methods yielded "normal" values of $E = 1.25$ eV and s between 4×10^{10} and 2×10^{12} s^{-1} in this material (see e.g. Yossian et al., 1993). However, peak-shape methods yielded very significantly higher values for the same peak. Taylor and Lilley (1978) reported on activation energy of 2.06 eV and a frequency factor of 2×10^{20} s^{-1}. Gorbics et al. (1967) communicated on $E = 2.4$ eV and $s = 1.7 \times 10^{24}$ s^{-1} and similar results were given by Bilski (2002). Pohlit (1969) reported on exceedingly high values of $E = 3.62$ eV and $s = 10^{42}$ s^{-1}. Also reported on experimentally found very high frequency factors Shinsho et al. (2005) who described the main glow peak in $CaSO_4$:Tm which was found to have $s = 10^{19}$ s^{-1}, and Bilski et al. (2008) who reported on $s = 5.6 \times 10^{28}$ s^{-1} in LiF:Mg,Cu,P. Another very narrow peak, with width of ~4 K for a glow peak at ~400 K in NaCl:KCl has been reported by Deshmukh et al. (1982), may also possibly be explained by the simultaneous two-electron transition. In this context, it should be mentioned that alternative methods have been proposed for the occurrence of very high activation energies and exceedingly high frequency factors. Chen and Hag-Yahya (1996) have used a model with three competing recombination centers, two of which are radiationless, that result in the mentioned features. A similar effect has been used by the same authors (Chen and Hag-Yahya, 1997) to explain the anomalous fading sometimes occurring in TL. Yet another explanation for the very high values has been given by Mandowski (2005), based on the concept of semi-localized transitions. The alternative model given here for the anomalously high effective frequency factor has been described in sub-section 4.3 above.

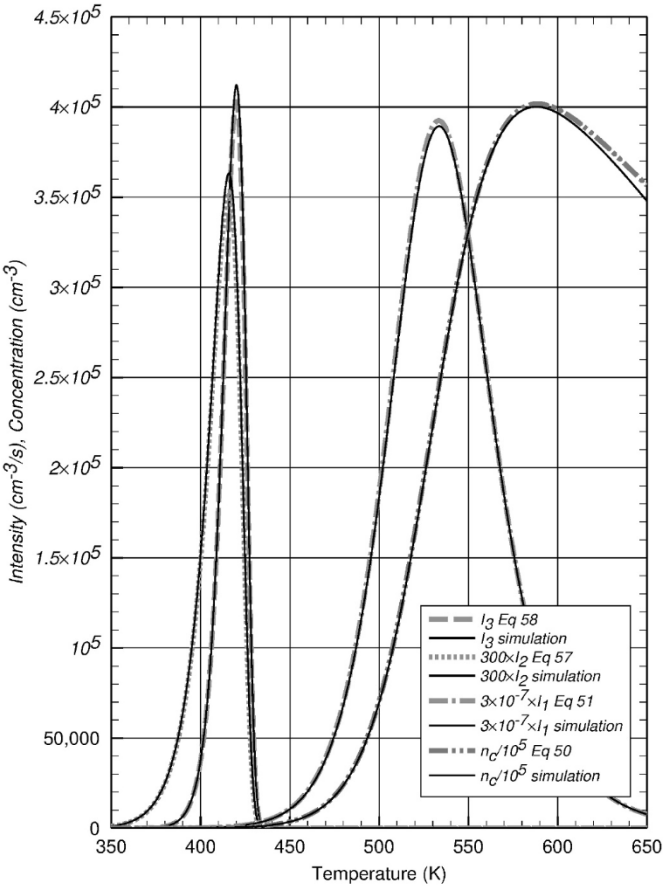

Fig. 7. Comparison of the simulated peaks of I_1, I_2, I_3 and n_c shown in Fig. 3 and the analytical approximate solutions described above. The meaning of the different line graphs is given in the inset.

The result that the peaks' intensities increase for decreasing values of A_d in curves (a-d) in Fig. 4 is anomalous at first sight. It appears that it can be ascribed to the process of excitation and even more so, the relaxation. During excitation and relaxation, more recombinations take place when A_d is larger which is translated to lower emission of TL during the heating stage.

As for the mentioned shift of the simulated TL peak to lower temperatures with the dose of excitation, it is usually considered to be a property of non-first-order peaks. In the present case, although the symmetry of the peaks resembles that of first-order curves, obviously the process is different and much more complex. Moreover, in the literature, are mentioned cases of first-order-looking peaks which shift toward lower temperature with increasing excitation dose. Miallier et al. (1991) reported the effect in quartz, Gastélum et al. (2007) reported it in diamond films and Nandha Gopal et al. (2016) in $CaSO_4$: Dy.

Regarding the results of Fig. 5, demonstrating a strongly skewed TL peak with symmetry factor below 0.3 (apparent order of kinetics significantly below unity), such experimental results have been reported in the literature. For example, Tiwari et al. (2014) have reported such peaks in UV irradiated ZrO_2:Ti phosphors. Tamrakar et al. (2015) have communicated on the same material with variable concentration of the dopant. Similar effect has been reported by Guntu et al. (2020) who communicated on such results in calcium fluoro borophosphate glass. Also should be mentioned the theoretical result by Halperin and Braner (1960) who demonstrated a similar effect following a different model. It should be noted that the dose used for the simulation of Fig. 5 is significantly higher than in the previous figures. This seems to be the reason for the unusual peak symmetry found (see below).

The results of Fig. 6 demonstrate the simulated dose dependence

which in this example has a slope a little higher than 2, which means more than quadratic dose dependence. The present explanation of such behavior is an alternative to previous possible explanations (see e.g. Chen et al., 1996, 2017, 2018; Lawless et al., 2019). As pointed out, the separation of the two lines of dose dependence by change of excitation intensity or excitation time indicates the possibility of dose-rate effect (see e.g. Horowitz et al., 2018).

Finally, the graphs shown in Fig. 7 demonstrate the very close agreement between the numerical simulations and the approximate analytical theory. The very small differences seen are attributed to the approximations made in the analytical development. As for the occurrence of strong asymmetry seen in Fig. 5, this does not agree with the results of the analytical approach simply because in the latter, relatively small excitation dose is assumed and in Fig. 5, rather high dose has been used.

Declaration of competing interest

The authors declare that they have no known competing financial interests or personal relationships that could have appeared to influence the work reported in this paper.

References

Baird, J.K., 1999. A generalized statement of the law of mass action. J. Chem. Educ. 76, 1146–1150.

Baldacchini, G., Pan, D.S., Lüty, F., 1981. Radiative and nonradiative processes of F and F' centers in NaBr and NaI. Phys. Rev. B24, 2174–2186.

Berezin, A.A., 1984. Instabilities against correlated two-electron tunnel transitions in impurity systems. Solid State Commun. 49, 87–89.

Betzler, K., Weller, T., 1971. Experimental evidence of two-electron transitions in solids. Phys. Rev. Lett. 26, 640–642.

Betzler, K., Weller, T., Conradt, R., 1972. Two-electron band-to-band transitions in solids. Phys. Rev. B6, 1394–1399.

Bilski, P., 2002. Lithium fluoride: from LiF:Mg,Ti to LiF:Mg, Cu,P. Radiat. Protect. Dosim. 100, 199–206.

Bilski, P., Obryk, B., Olko, P., Mandowska, E., Mandowski, A., Kim, J.L., 2008. Characteristics of LiF:Mg,Cu,P in ultra-high dose range. Radiat. Meas. 43, 315–318.

Böhm, M., Scharmann, A., 1981. In: Oberhofer, M., Scharmann, A. (Eds.), Theory, *Applied Thermoluminescence Dosimetry*, pp. 11–38. Ch. 2.

Bowman, S.G.E., Chen, R., 1979. Superlinear filling of traps in crystals due to competition during heating. J. Lumin. 18/19, 345–348.

Burbaev, T.M., Kozyrev, D.S., Sibedlin, N.N., Skorikov, M.L., 2013. Luminescence of a quasi-two-dimensional electron-hole liquid and excitonic molecules in Si/SiGe/Si heterostructures upon two-electron transitions. JETP Lett. (Engl. Transl.) 98, 823–828.

Chen, R., 1969. On the calculation of activation energies and frequency factors from glow curves. J. Appl. Phys. 40, 570–585.

Chen, R., 1971. Simultaneous measurements of thermally stimulated conductivity and thermoluminescence. J. Appl. Phys. 42, 5899–5901.

Chen, R., Fogel, G., 1993. Superlinearity in thermoluminescence revisited. Radiat. Protect. Dosim. 47, 23–26.

Chen, R., Fogel, G., Lee, C.K., 1996. A new look at the models of the superlinear dose dependence of thermoluminescence. Radiat. Protect. Dosim. 65, 63–68.

Chen, Hag-Yahya, A., 1996. Investigation of very high activation energies and frequency factors as being due to competition between centres. Radiat. Protect. Dosim. 65, 17–20.

Chen, R., Hag-Yahya, A., 1997. A possible new interpretation of the anomalous fading in thermoluminescent materials as normal fading in disguise. Radiat. Meas. 27, 205–210.

Chen, R., Lawless, J.L., Pagonis, V., 2017. Thermoluminescence associated with two-electron traps. Radiat. Meas. 99, 10–17.

Chen, R., Lawless, J.L., Pagonis, V., 2018. Thermoluminescence associated with two-hole recombination centers. Radiat. Meas. 115, 1–6.

Chen, R., Yang, X.H., McKeever, S.W.S., 1988. The strongly superlinear dose dependence of thermoluminescence in synthetic quartz. J. Phys. D Appl. Phys. 21, 1452–1457.

Dean, P.J., Cuthbert, J.D., Thomas, D.G., Lynch, R.T., 1967. Two-electron transitions in the luminescence of excitons bound to neutral donors in gallium phosphide. Phys. Rev. Lett. 18, 122–124.

Deshmukh, B.T., Pode, R.B., Moharil, S.V., 1982. Anomalous thermoluminescent emission from NaCl:KCl crystals. Phys. Rev. B25, 7520–7522.

Eliyahu, I., Druzhyna, S., Horowitz, Y., Reshes, G., Biderman, S., Oster, L., 2016. Kinetic simulation of charge transfer following 5.08 eV (F band) optical excitation of irradiated LiF:Mg,Ti (TLD-100): participation of holes released via V_3-V_k transformation. Radiat. Meas. 90, 27–32.

Ferner, R.E., Aronson, J.K., 2016. Cato guldenberg and peter waage, the history of the law of mass action, and its relevance to clinical pharmacology. Br. J. Clin. Pharmacol. 81, 51–55.

Gastélum, S., Cruz-Zaragoza, E., Meléndrez, R., Chernov, V., Barboza-Flores, M., 2007. Dose rate effects on the thermoluminescence properties of MWCVD diamond films. Radiat. Eff. Defect Solid 162, 587–595.

Gorbics, S.G., Attix, F.H., Pfaff, J.A., 1967. Temperature stability of CaF_2:Mn and LiF (TLD-100) thermoluminescent dosimeters. Int. J. Appl. Radiat. 18, 625–630.

Guldberg, C.M., Waage, P., 1864. Etudes sur les affinités. Les Mondes 12, 107–113.

Guntu, R.K., Jahangeer, N., Rao, Ch S., 2020. Thermoluminescence, elastic and dielectric investigations of calcium fluoro borophosphate glass composite materials doped by small concentrations of TiO_2. Indian J. Phys. https://doi.org/10.1007/s12648-020-01720-8.

Halperin, A., Braner, A.A., 1960. Evaluation of thermal activation energies from glow curves. Phys. Rev. 117, 408–415.

Halperin, A., Chen, R., 1966. Thermoluminescence of semiconducting diamonds. Phys. Rev. 148, 839–845.

Hinkley, S.W., Tsokos, C.P., 1974. A stochastic model for chemical equilibrium. Math. Biosci. 21, 85–102.

Horowitz, Y., 2006. A unified and comprehensive theory of the TL dose response of thermoluminescent systems applied to LiF:Mg,Ti. In: Horowitz, Y. (Ed.), Microdosimetric Response of Physical and Biological Systems to Low- and High-LET Radiations. Elsevier, Amsterdam, pp. 75–202.

Horowitz, Y., Oster, L., Eliyahu, I., 2018. Review of dose-rate effects in the thermoluminescence of LiF:Mg,Ti (Harshaw). Radiat. Protect. Dosim. 179, 184–188.

Kristianpoller, N., Chen, R., Israeli, M., 1974. Dose dependence of thermoluminescence peaks. J. Phys. D Appl. Phys. 7, 1063–1072.

Lawless, J.L., Chen, R., Pagonis, V., 2019. Thermoluminescence governed by the Auger-recombination process. Radiat. Meas. 124, 40–47.

Lund, E.W., 1965. Guldberg and Waage and the law of mass action. J. Chem. Educ. 42, 548–550.

Mandowski, A., 2005. Semi-localized transitions model for thermoluminescence. J. Phys. D Appl. Phys. 38, 17–21.

Mayhugh, M.R., 1970. Color centers and the thermoluminescence mechanism in LiF. J. Appl. Phys. 41, 4776–4782.

Miallier, D., Faïn, J., Montret, Th, Sanzelle, S., Soumana, S., 1991. Properties of the red TL peak of quartz relevant to thermoluminescence dating. Nucl. Tracks Radiat. Meas. 18, 89–94.

Nandha Gopal, J., Sanyal, Bhaskar, Lakshmanan, Arunachalam, 2016. Thermoluminescence of high sensitive microcrystalline $CaSO_4$:Dy for high dose measurements. Int. J. Lumin. Appl. 6, 14–19.

Otaki, H., Kido, H., Hiratsuka, A., Fukuda, Y., Takeuchi, N., 1994. Estimation of UV radiation dose using CaF_2:Tb_4O_7 as a thermoluminescence dosimeter. J. Mater. Sci. Lett. 13, 1267–1269.

Pohlit, W., 1969. Thermoluminescence in LiF. I. Measurement of activation energy of electrons in different traps. Biophysik 5, 341–350.

Porret, F., Lüty, F., 1971. Luminescence and F' formation involving spin-polarized F centers in KCl. Phys. Rev. Lett. 26, 843–846.

Shinsho, K., Suzuki, Y., Yamamoto, Y., Urushiyama, A., 2005. The thermoluminescence activation energy and frequency factor of the main glow of $CaSO_4$:Tm phosphor determined by heating rate method including very slow rates of heating. J. Appl. Phys. 97 (1–4), 123523.

Tamrakar, R.K., Tiwari, N., Kuraria, R.K., Bisen, D.P., Dubey, V., Upadhyay, K., 2015. Effect of annealing temperature on thermoluminescence glow curve for UV and gamma ray induced ZrO_2:Ti phosphor. J. Radiat. Res. Appl. Sci. 8, 1–10.

Taylor, G.C., Lilley, E., 1978. The analysis of thermoluminescent glow peaks in LiF(TLD-100). J. Phys. D: Appl. Phys. 11, 567–581.

Tiwari, N., Kuraria, R.K., Tamrakar, R.K., 2014. Thermoluminescence glow curve for UV induced ZrO_2:Ti phosphor with variable concentration and various heating rate. J. Radiat. Res. Appl. Sci. 7, 542–549.

Townsend, P.D., Taylor, G.C., Wintersgill, M.C., 1979. An explanation of the anomalously high activation energies of TL in LiF (TLD 100). Radiat. Eff. 41, 11–16.

Wagner, H.P., Lankes, S., Wolf, D., Lichtenberger, D., Kuhn, P., Gebhardt, W., 1992. Resonant excitation of intrinsic and shallow trap luminescence in MOVPE grown ZnTe layers. J. Lumin. 52, 41–53.

Winter, E.M., Wolfe, D.R., Christy, R.W., 1969. Dichroism of V bands in potassium and rubidium halides. Phys. Rev. 186, 949–952.

Woda, C., Wagner, G.A., 2007. Non-monotonic dose dependence of the Ge- and Ti-centers in quartz. Radiat. Meas. 42, 1441–1452.

Yazici, A.N., Karali, T., Townsend, P.D., Ari, M., 2004. Thermoluminescence studies of LiF:Mg,Ti between 100 and 300 K. J. Phys. D Appl. Phys. 37, 3165–3173.

Yossian, D., Mahajna, S., Ben-Shachar, B., Horowitz, Y.S., 1993. Re-investigation of the kinetic trapping parameters of peak 5 in TLD-100 via 'prompt' and 'residual' isothermal decay. Radiat. Protect. Dosim. 47, 129–133.

Zhang, G.G., Leung, G.H., Song, K.S., 1994. Two-electron defect systems in ionic crystals: application to F' centers in alkali halides. J. Phys.: Condens. Matter 6, 7715–7723.